Observation of asymmetric fission in ^{204}Pb at low excitation energies

Vineet Kumar,[1,2] K. Mahata ®,[1,2,*] Sangeeta Dhuri ®,[1,2] A. Shrivastava,[1,2] K. Ramachandran,[1] S. Pandit,[1,2] V. V. Parkar,[1,2] Arati Chavan,[3] Abhinav Kumar,[1] Satbir Kaur,[1,2] and P. C. Rout[1,2]

[1]*Nuclear Physics Division, Bhabha Atomic Research Centre, Mumbai 400085, India*
[2]*Homi Bhabha National Institute, Anushaktinagar, Mumbai 400094, India*
[3]*Vivekanand Education Society's College of Arts, Science and Commerce, Mumbai 400071, India*

The fragment mass and total kinetic energy distributions were measured in fission of ^{204}Pb, populated in the ^{7}Li + ^{197}Au reaction at excitation energies down to 15.3 MeV above the fission barrier. Fits considering admixture of symmetric and asymmetric fission indicate the presence of substantial asymmetric fission at all measured energies. The measured mass distributions are in good agreement with the model predictions. The observed excitation energy dependence of asymmetric fission fractions for the present system is compared with those for near−by nuclei and predictions of theoretical models to understand the damping of shell correction at large deformation.

I. INTRODUCTION

Nuclear fission, discovered in 1938 [1], represents one of the most substantial cases of nuclear transformation. In this process a heavy nucleus splits into two fragments, releasing a large amount of energy. The gross features of the fission process could be described within the simplistic liquid-drop (LD) model [2,3]. In this macroscopic approach, the shape-dependent surface and Coulomb energy terms define a smoothly varying potential-energy landscape through which fission occurs. However, it predicts symmetric fragment mass distributions and could not explain the observed asymmetric mass splits of actinides. Incorporation of shell corrections to the liquid drop potential energy was necessary to understand the asymmetric nature of the mass split [4]. The fission fragment mass distribution is one of the best observables to understand fission mechanisms as it is sensitive to the variation in the nuclear potential energy surface, particularly at lower excitation energies. Even though much progress has taken place, a comprehensive understanding of this complex process is yet to be achieved, and it continues to be a subject of active debate [5–7].

Particularly, fission of preactinide nuclei is sparsely investigated owing to very low fission probability. Signature of asymmetry in light-ion induced fission of preactinides near the β-stability line was first reported in the 1980s [8]. Recent observation of dominantly asymmetric mass distribution in β-delayed fission of the neutron-deficient ^{180}Hg isotope at excitation energy just above the fission barrier [9] prompted a renewed theoretical and experimental interest in the fission of nuclei in this region. The number of systems that can be studied in β-delayed fission are limited. Though the

structure effects are significantly diminished at moderately higher excitation energies populated in heavy-ion reactions, they have been found to be suitable to extend the investigation of asymmetric fission over a broader region. In most of the cases, heavier projectiles ($A \geqslant 35$) have been used as they allow access to the more neutron deficient region [10–17]. All these studies have firmly demonstrated the presence of asymmetric fission in the preactinide region.

In a systematic study [18], it was revealed that the mean value of Z of the light fragment, evaluated assuming unchanged charge density (UCD) [19], varies less as compared to that of the heavy fragment with Z the fissioning nuclei. No preferential population of neutron number was observed. Thus, it was concluded that the light fragment proton shells with $Z \approx 36$ provide the stabilization in asymmetric fission of preactinide nuclei. In a recent study of the mass and total kinetic energy (TKE) distributions, an independent mode of stabilization in the heavy fragment was conjectured [10]. However, the simultaneous mass-TKE fit has ruled-out the necessity of additional stabilization in the heavy fragment [12].

The attempts to explain the new type of asymmetric fission include shell effects in the pre-scission configurations associated with dinuclear structures or octupole deformed shells in the nascent fragments and fissioning nucleus [18,20–23]. The predictions of the Brownian shape motion (BSM) on a five-dimensional potential-energy surface are available for a large number of nuclei [24]. The asymmetric saddle point, manifested in the calculated five-dimensional potential-energy surface, was associated to the neutron shell configurations of the fissioning nuclei, and was identified to drive the asymmetric mass distribution in this region. The GEF (general description of fission observables) [25], a semiempirical framework, was also found to provide good description of the available experimental data in this mass region [18]. This
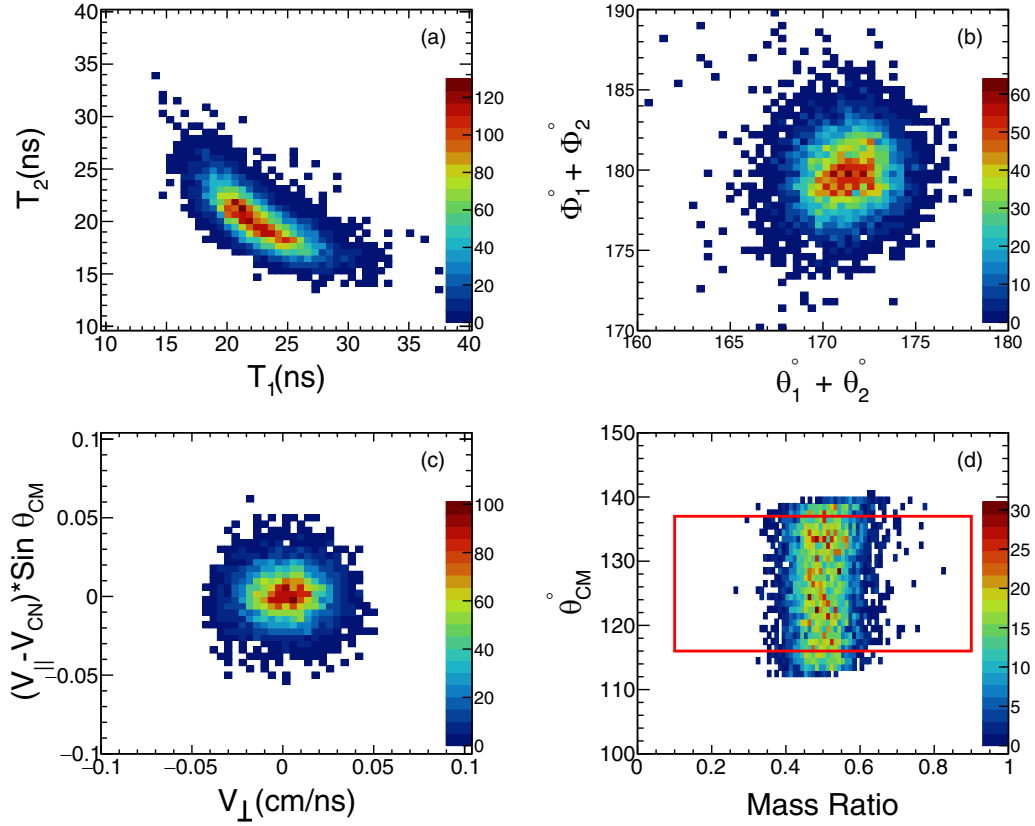
*kmahata@barc.gov.in

FIG. 1. Correlation between the (a) time of flights (T_1 and T_2), (b) folding angle ($\theta_1 + \theta_2$) and total azimuthal angle ($\phi_1 + \phi_2$), (c) parallel ($v_\parallel$) and perpendicular ($v_\perp$) components of velocity, and (d) mass ratio and emission angle in the center of mass frame ($\theta_{\text{c.m.}}$) of fission fragments for ^{7}Li + ^{197}Au reaction at $E^*_{\text{SP}} = 18.4$ MeV.

model includes a asymmetric fission mode with $Z \approx 36$. In a recent study [26], the experimental mass distributions for ^{187}Ir were found to differ from the predictions of the above models, emphasizing the need for further studies.

Investigations have also shown that there is a substantial presence of quasifission, an entrance channel dependent phenomena, in reactions involving projectiles with mass $A \geqslant 35$ in this mass region [27]. The fission fragment mass distributions in reactions involving projectiles with mass $A \geqslant 35$ were found to be broader than those corresponding to more asymmetric entrance channels. As quasifission occurs before complete equilibration of mass, it can lead to enhanced population of the asymmetric fission fragments. Thus more rigorous treatment involving dynamics is required to interpret the data for the more symmetric entrance channels. On the other hand, the asymmetric entrance channels can be used to investigate the role of shell structure. At present, asymmetric fission studies at moderate excitation energies in this mass region utilizing more asymmetric entrance channels are limited [26–29] and more studies can help to understand the mechanism of asymmetric fission in the preactinide region.

The present paper reports the study of fission fragment mass and TKE distributions to investigate the presence of asymmetric fission mode(s) at moderate excitation energy for ^{204}Pb, populated in the ^{7}Li + ^{197}Au reaction. The paper is structured as follows. Experimental details and data analysis procedures are presented in Sec. II. The characteristics of the

experimental fission fragment mass and TKE distributions are discussed in Sec. III along with the comparisons to model calculations. The summary and conclusions are then presented in Sec. IV.

II. EXPERIMENTAL DETAILS AND DATA ANALYSIS

The experiment was carried out at the BARC-TIFR Pelletron-LINAC facility Mumbai, India. A 280 μg/cm^2 thick self-supporting target of ^{197}Au was bombarded with pulsed ^{7}Li beams of energies 30, 35, and 42 MeV. Two large area (12.5×7.5 cm^2) multiwire proportional counters (MWPCs)

TABLE I. The excitation energies of the compound nucleus ($E^\star$) along with the statistical model [35,36] estimates for the mean angular momentum of the fissioning nucleus ($\langle \ell_{\text{fiss}} \rangle$), prefission neutron multiplicity (ν_{pre}), average energy removed by neutron emission (E_{pre}), and the excitation energies above the saddle point ($E^\star_{\text{SP}}$) are listed. Total fission events collected at each energies are also mentioned.

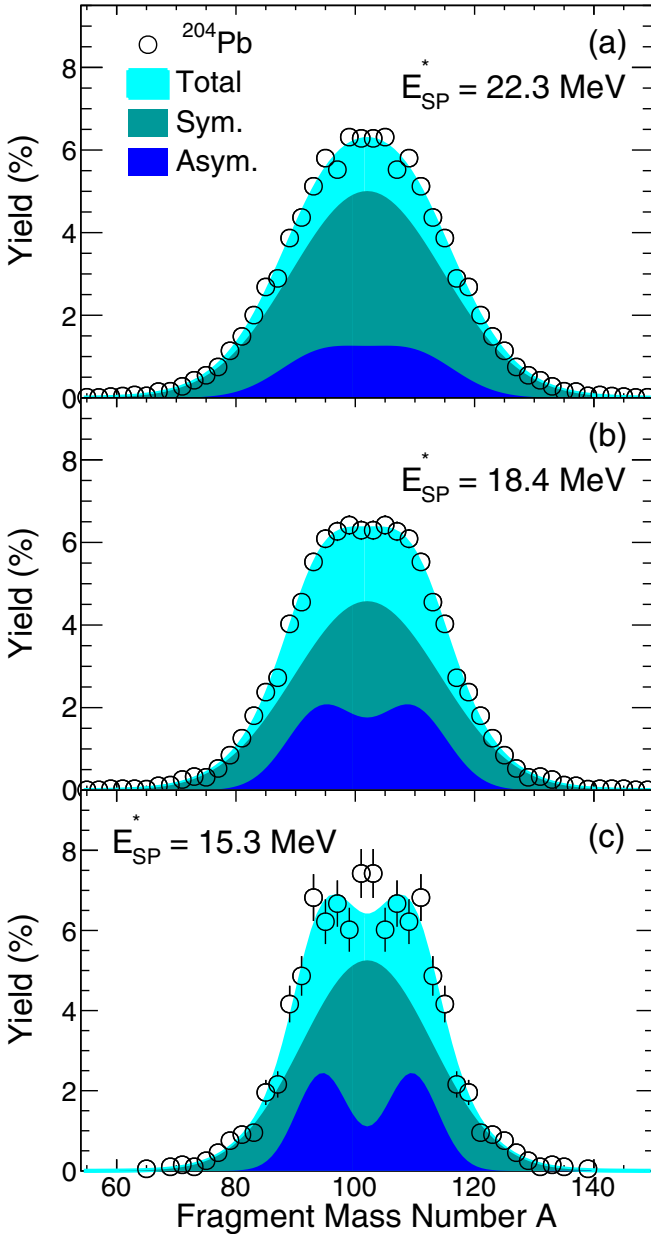| $E^\star$ (MeV)	$\langle \ell_{\text{fiss}} \rangle$ ($\hbar$)	ν_{pre}	E_{pre} (MeV)	$E^\star_{SP}$ (MeV)	Total counts
49.4	16.1	0.5	4.8	22.3	57180
42.7	11.1	0.2	2.2	18.4	11488
37.9	7.1	0.1	0.6	15.3	2166

FIG. 2. The measured fission fragment mass distributions of ^{204}Pb in the ^{7}Li + ^{197}Au reaction. The results of the multi-Gaussian fit to extract symmetric and asymmetric fission fractions are also shown.

FIG. 3. The measured fission fragment mass distributions for ^{204}Pb in the ^{7}Li + ^{197}Au reaction are compared with the predictions of the semiempirical GEF model [25]. The GEF predictions are smeared with the experimental mass resolution ($\sigma \approx 3u$) for direct comparisons with the measured data

[30] were placed at a distance of 24 cm from the target in a scattering chamber of diameter 1.5 m at $-50°$ and $121.5°$ for the coincident detection of the fission fragments. From each detector, one timing and four position signals (two each of X and Y coordinates) were fed into time to digital converter (TDC) after incorporating appropriate delays. The trigger or start signal was generated by making an "AND" gate of radiofrequency (RF) signal, associated with the beam pulse from the accelerator, with the output of the "OR" gate of timing signals from MWPCs. Two silicon surface barrier detectors were placed at $\pm 20°$ to monitor the beam quality by detecting the elastically scattered beam particles.
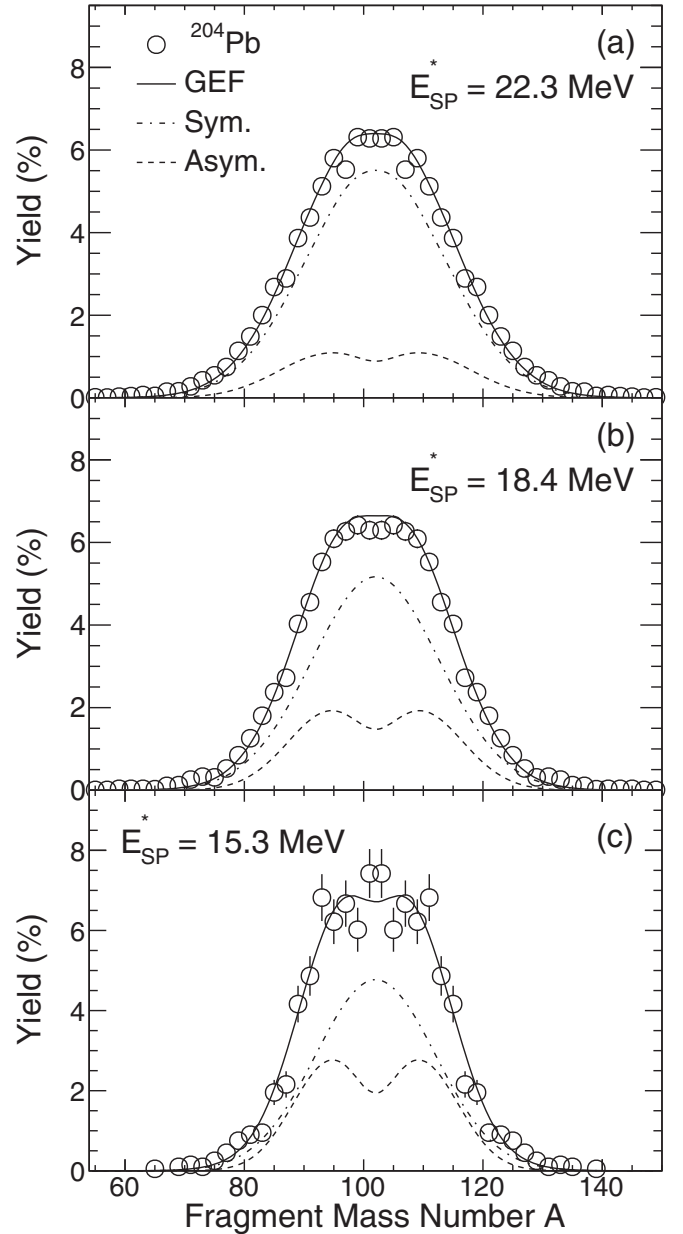
The data were acquired in an event by event mode using a VERSA-Module Euro card (VME) based multiparameter data-acquisition system [31]. The setup gave access to the position of detection (x_1, y_1, x_2, y_2,) and energy loss (ΔE_1, ΔE_2) of the fragments in the detectors, as well as their time of flight (T_1, T_2) with respect to the beam pulse. At the lowest energy, the beam pulsing was switched off to maximize the current, and thus only the time difference $\Delta T = (T_1 - T_2)$, instead of individual time of flights, was recorded.

The time of flight and position information were used to determine the fragment velocities. The emission angles,
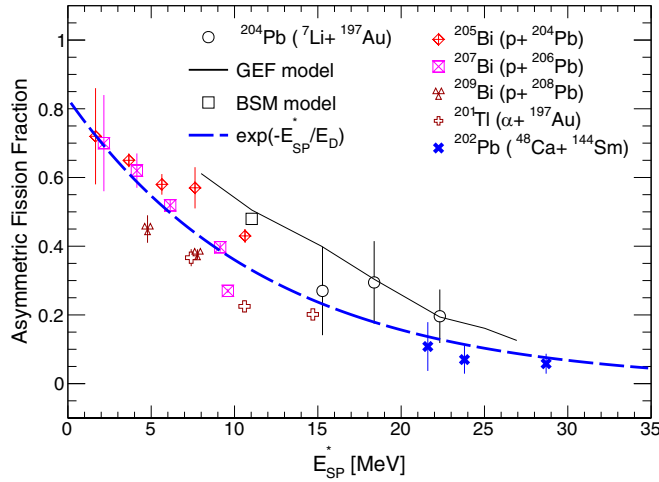
FIG. 4. The measured asymmetric fission fractions for ^{204}Pb are compared with the predictions of the GEF [25] and BSM models [24] as a function of excitation energy at the saddle point. The experimental asymmetric fission fractions are also compared with results for nearby nuclei (^{202}Pb [10], ^{201}Tl [28], and ^{205,207,209}Bi [29]) are also shown for comparison. The blue dashed line corresponds to a fit considering all the data points with an exponentially falling function [$\exp(-E^*_{SP}/E_D)$] with $E_D = 12$ MeV.

and azimuthal angles, as well as between the parallel and perpendicular components of the velocity onto the beam axis, were constructed to confirm the binary nature of the reaction. Preneutron fragment masses were finally determined using the time-of-flight (TOF) difference method. Small corrections in the fragment masses due to their energy loss in the target were obtained on an event-by-event basis in an iterative manner, taking the energy loss information from SRIM [33] for all possible fragments. The TKE was obtained using the the relation TKE $= 0.5 \, M_{CN} v_1 v_2$, where M_{CN} is the mass of the compound nucleus and $v_1 v_2$ is the product of the velocities of the fragments in the center of mass.

Figure 1 shows representative correlation plots used to select binary fission events corresponding to $E^*_{SP} = 18.4$ MeV. As shown in Fig. 1(a), the correlation in the TOFs (T_1 vs. T_2) allowed clear separation of the fission events from other reaction channels (not seen in the plot). The folding angle ($\theta_1 + \theta_2$) and total azimuthal angle ($\phi_1 + \phi_2$) distributions [Fig. 1(b)] are observed to peak at the estimated angle according to the Viola systematics [34] and 180°, respectively. The correlation between parallel and perpendicular components of the velocities onto the beam axis, shown in Fig. 1(c), confirms the binary nature of the reaction. Further, the absence of any correlation between the fragment mass (A) and the emission angle ($\theta_{c.m.}$) [Fig. 1(d)] rules out any significant presence of noncompound fission process in the present case. The events inside the graphical cut, shown in Fig. 1(d), are used for the further analysis to remove the detector edge effects.
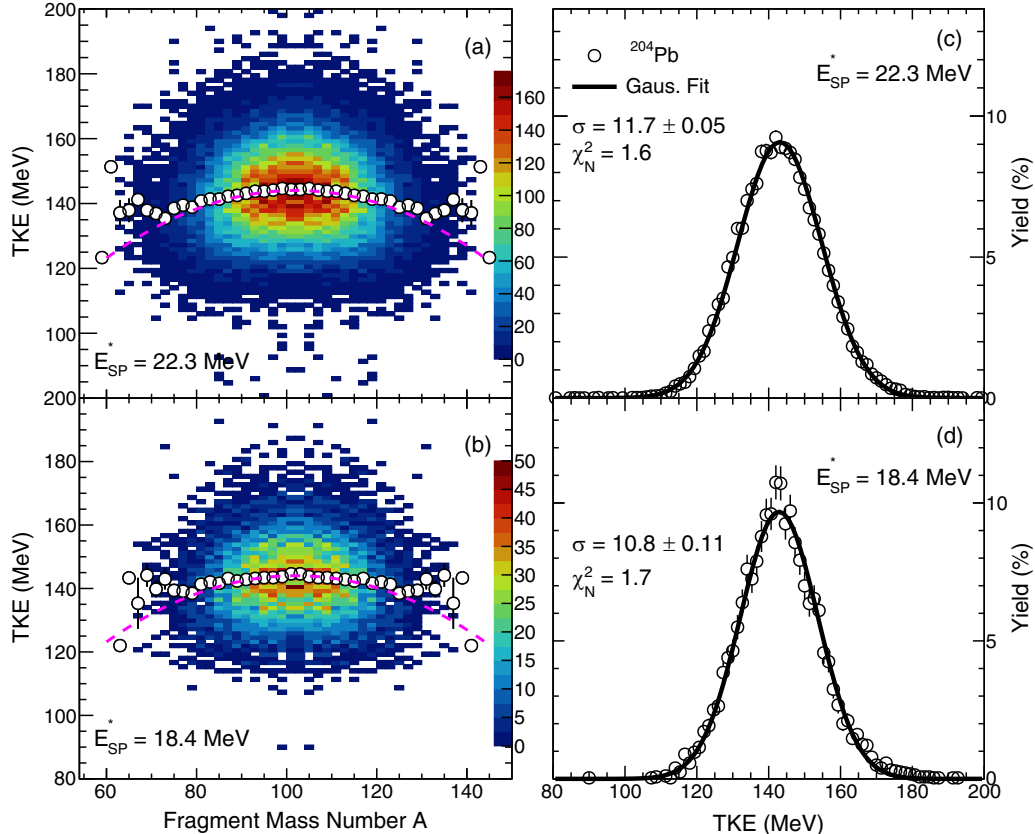
calculated from the position information, were used to obtain the linear momenta [32]. The correlations between the folding

FIG. 5. The measured fragment mass-TKE correlations along with TKE profiles (white filled circles) for ^{204}Pb. The magenta dashed line is the LD-predicted mass dependence of TKE [34]. (c) and (d) show the measured TKE distributions along with the Gaussian fits.

III. RESULTS AND DISCUSSION

The excitation energies ($E^\star$) of the compound nucleus along with the statistical model estimates for the mean angular momentum of the fissioning nuclei ($\langle \ell_{\text{fiss}} \rangle$), pre-fission neutron multiplicity (ν_{pre}), the average energy removed by the prefission neutrons (E_{pre}), and the excitation energies of the formed CN at the saddle point ($E^\star_{\text{SP}}$) are listed in Table. I. The statistical model estimates were obtained using the Monte Carlo code PACE [35] with a consistent prescription for the fission barrier and level density [36].

The measured fission fragment mass distributions are presented in Fig. 2. The experimental fission fragment mass distributions could be fitted well with the sum of symmetric and asymmetric components. The yields and widths of symmetric and asymmetric components were the free parameters for the fitting procedure. The peak position for the symmetric component was kept fixed at $A_{\text{CN}}/2$ as expected from the liquid drop (LD) model. From the systematics, the position for light fragment peak is expected at $Z = 38$ [18] as the corresponding neutron number is larger than 50. The mass number of the light fragment peak was evaluated under the UCD assumption. As the counts of the complementary fragments are completely correlated, the fitting range was restricted below $A_{\text{CN}}/2$. The symmetric and asymmetric components along with the total fit function are shown in Fig. 2. From the fits, substantial presence of asymmetric fission could be found at all the measured energies. As expected, the shell correction driven asymmetric component was observed to diminish with increase in excitation energy.

The predictions of the GEF model [25], folded with the experimental mass resolution ($\sigma = 3\,\text{u}$), are compared with the measured fission fragment mass distributions in Fig. 3. The GEF model gives a good description of the measured data. It also predicts substantial asymmetric contribution at all three energies and a gradual reduction of the asymmetric component. The predictions of the BSM model [24] are not available in the same E^* range. Thus the measured mass distributions could not be compared quantitatively. However, the observed peak position of the light fragment ($A_L \approx 95$) agrees well with the prediction of the BSM model. It is important to note here that the experimental mass distributions for ^{187}Ir [26] were found to differ significantly from the predictions of different models, particularly the BSM model.

Asymmetric fission fractions (the ratios of the asymmetric yield/total yield) obtained from the fits to the experimental mass distributions for ^{204}Pb are plotted as a function of excitation energy at the saddle point in Fig. 4. This fraction is directly related to the surviving shell correction at a given excitation energy. The measured asymmetric fission fractions are in good agreement with the predicted trend of the GEF model [25]. Moreover, the predicted asymmetric fraction from the BSM model [24], available at slightly lower energy, was found to agree with the observed trend in the experimental data and GEF prediction. The contributions of asymmetric fission for ^{204}Pb are also compared with those for nearby systems, namely ^{202}Pb [10], ^{201}Tl [28], and ^{205,207,209}Bi [29]. As anticipated, the fraction of asymmetric fission decreases as the excitation energy at the saddle point increases for all the

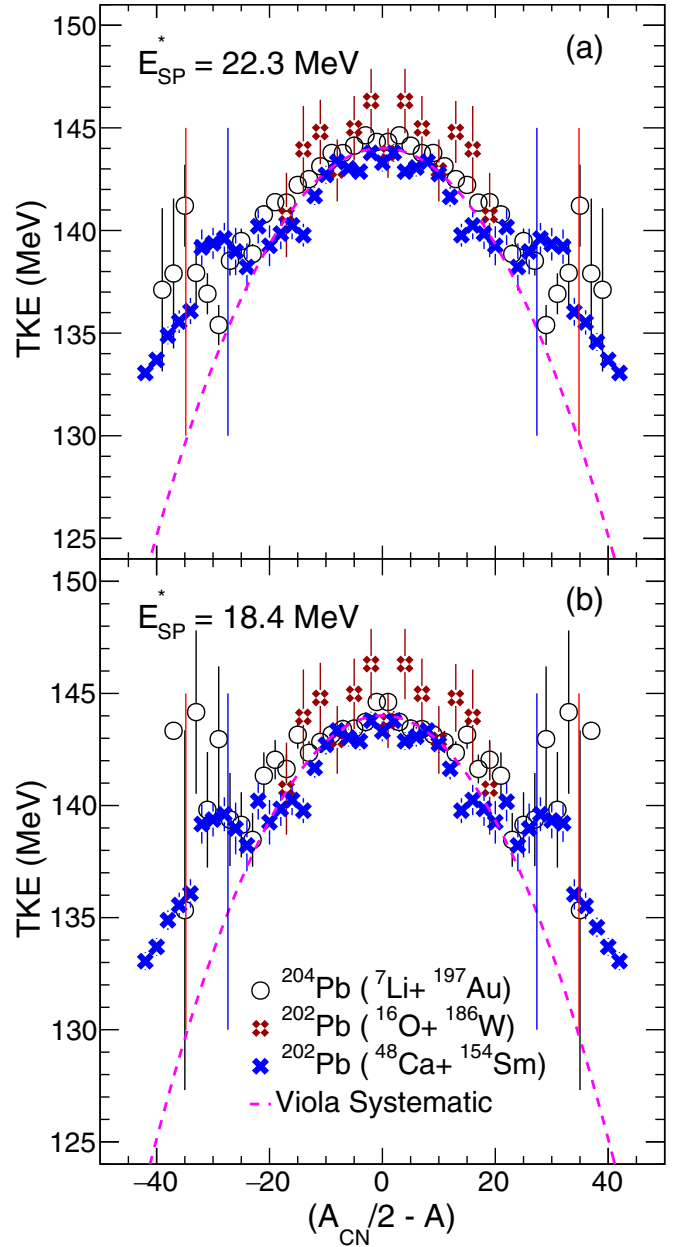FIG. 6. The TKE profiles for ^{204}Pb from the present measurement are compared with those for ^{202}Pb [41] measured in the ^{16}O and ^{48}Ca induced reactions at $E^\star_{\text{SP}} = 23$ and 24 MeV, respectively. The blue and red vertical lines show the position of fragments with mass corresponding to $Z = 52$ and $Z = 55$ assuming an unchanged charge distribution from compound nucleus to fragments.

systems considered. The excitation energy dependence could be described well using an exponentially falling function, $\exp(-E^\star_{\text{SP}}/E_D)$ with a damping parameter, $E_D = 12\,\text{MeV}$. It is interesting to note that a similar damping parameter provides good description of the asymmetric fraction data available for an actinide nuclei, ^{236}U at a similar excitation energy range [37]. Further, the present damping factor is found to be faster then that obtained from level density studies for the equilibrium deformation [38,39].

The measured correlations between fragment mass and total kinetic energy (TKE) for ^{204}Pb at $E_{SP}^* = 22.3$ MeV and $E_{SP}^* = 18.4$ MeV are presented in Fig. 5, along with the TKE profiles (white filled circles). The magenta dashed lines represent the mass dependence of TKE as predicted by the liquid drop model [34]. The measured TKE profiles agree well with the LD-predicted mass dependence of TKE. In panels (c) and (d) of Fig. 5, the measured distributions of TKE for ^{204}Pb at $E_{SP}^* = 22.3$ MeV and $E_{SP}^* = 18.4$ MeV are depicted. These distributions could be fitted well with a single Gaussian function. The observed widths of the TKE distributions, 11.7 ± 0.05 MeV and 10.8 ± 0.11 MeV for $E_{SP}^* = 22.3$ MeV and 18.4 MeV, respectively, are in good agreement with systematics [11,40] based on liquid drop behavior. Thus, the measured TKE distributions do not reveal much about the mechanism of fission in the present case. In Ref. [11], the measured TKE distributions were found to be sensitive to fission modes and their widths were observed to be larger than the expectations from the systematics based on LD behavior for the neutron deficient nuclei studied.

The TKE profiles from the present measurement are compared with those for ^{202}Pb populated at $E_{SP}^* = 23$ and 24 MeV in ^{16}O + ^{186}W and ^{48}Ca + ^{154}Sm reactions [41], respectively, in Fig. 6. The widths of the mass distributions for ^{16}O + ^{186}W and those of the central part of mass distributions for ^{48}Ca + ^{154}Sm systems could be explained simultaneously using the statistical relation, an indication of fully equilibrated compound nuclear decay. However, asymmetric shoulders peaked around masses 65 and 140 were observed in the mass distributions for the ^{48}Ca + ^{154}Sm system, particularly at lower excitation energies. The TKE profile also showed a deviation from the parabolic behavior in that region. The present system also shows deviation from the parabolic dependence at the same place, though no significantly enhanced population could be observed in the measured mass distributions as shown in Fig. 2. As it appears around $Z = 52$–55 (shown as blue and red vertical lines), this deviation could be attributed to standard fission modes prominently observed in the actinide region.

IV. SUMMARY

To summarize, this study focused on the measurement of fission fragment mass and total kinetic energy distributions for ^{204}Pb, which was populated through the ^{7}Li + ^{197}Au reaction. The measured mass distributions of ^{204}Pb could be reproduced well using a combination of symmetric and asymmetric components. The symmetric and asymmetric contributions were extracted for all excitation energies of the compound nucleus.

The analysis revealed that the fission fragment mass distributions have significant contribution from the asymmetric fission mode at all three measured excitation energies. The GEF model reproduced the measured mass distributions and the corresponding asymmetric fractions well. The extracted values of the asymmetric fission fraction vary from 20% to 27% in the measured energy range. Furthermore, the observed decrease in the shell effect driven asymmetric fission fraction with increasing excitation energy is found to be similar to those for the nearby fissioning nuclei. The predictions of both the GEF and BSM models are also in good agreement with the observed experimental trend. Unlike the behavior observed in lighter preactinides [26,42], the experimental observations for the heavier preactinides could be effectively reproduced by the existing models.

The TKE profiles show deviations from the LD behavior around the standard fission modes ($Z = 52$–55) as observed in heavier preactinides earlier [8,41]. Unlike the observed peculiarities in some of the neutron deficient light preactinides [10,11], the measured distributions of total kinetic energy and their profile do not show any departure from LD expectations corresponding to the new asymmetric mode(s).

[1] O. Hahn, L. Meitner, and F. Strassmann, Ber. dtsch. Chem. Ges. A/B **70**, 1374 (1937).

[2] N. Bohr and J. A. Wheeler, Phys. Rev. **56**, 426 (1939).

[3] L. Meitner and O. R. Frisch, Nature (London) **143**, 239 (1939).

[4] V. M. Strutinsky, Nucl. Phys. A **95**, 420 (1967).

[5] A. N. Andreyev, K. Nishio, and K.-H. Schmidt, Rep. Prog. Phys. **81**, 016301 (2018).

[6] K.-H. Schmidt and B. Jurado, Rep. Prog. Phys. **81**, 106301 (2018).

[7] S. Kailas and K. Mahata, Pramana - J. Phys. **83**, 851 (2014).

[8] M. G. Itkis, V. N. Okolovich, and A. Y. Rusanov, Z. Phys. A **320**, 433 (1985).

[9] A. N. Andreyev, J. Elseviers, M. Huyse, P. Van Duppen, S. Antalic, A. Barzakh, N. Bree, T. E. Cocolios, V. F. Comas, J. Diriken, D. Fedorov, V. Fedosseev, S. Franchoo, J. A. Heredia, O. Ivanov, U. Köster, B. A. Marsh, K. Nishio, R. D. Page, N. Patronis *et al.*, Phys. Rev. Lett. **105**, 252502 (2010).

[10] A. A. Bogachev, E. M. Kozulin, G. N. Knyazheva, I. M. Itkis, M. G. Itkis, K. V. Novikov, D. Kumar, T. Banerjee, I. N. Diatlov, M. Cheralu, V. V. Kirakosyan, Y. S. Mukhamejanov,

A. N. Pan, I. V. Pchelintsev, R. S. Tikhomirov, I. V. Vorobiev, M. Maiti, R. Prajapat, R. Kumar, G. Sarkar *et al.*, Phys. Rev. C **104**, 024623 (2021).

[11] E. M. Kozulin, G. N. Knyazheva, I. M. Itkis, M. G. Itkis, Y. S. Mukhamejanov, A. A. Bogachev, K. V. Novikov, V. V. Kirakosyan, D. Kumar, T. Banerjee, M. Cheralu, M. Maiti, R. Prajapat, R. Kumar, G. Sarkar, W. H. Trzaska, A. N. Andreyev, I. M. Harca, A. Mitu, and E. Vardaci, Phys. Rev. C **105**, 014607 (2022).

[12] B. Swinton-Bland, J. Buete, D. Hinde, M. Dasgupta, T. Tanaka, A. Berriman, D. Jeung, K. Banerjee, L. Bezzina, I. Carter, K. Cook, C. Sengupta, C. Simenel, E. Simpson, and M. Stoyer, Phys. Lett. B **837**, 137655 (2023).

[13] R. Tripathi, S. Sodaye, K. Sudarshan, B. K. Nayak, A. Jhingan, P. K. Pujari, K. Mahata, S. Santra, A. Saxena, E. T. Mirgule, and R. G. Thomas, Phys. Rev. C **92**, 024610 (2015).

[14] E. Prasad, D. J. Hinde, K. Ramachandran, E. Williams, M. Dasgupta, I. P. Carter, K. J. Cook, D. Y. Jeung, D. H. Luong, S. McNeil, C. S. Palshetkar, D. C. Rafferty, C. Simenel, A. Wakhle, J. Khuyagbaatar, C. E. Düllmann, B. Lommel, and B. Kindler, Phys. Rev. C **91**, 064605 (2015).

[15] K. Nishio, A. Andreyev, R. Chapman, X. Derkx, C. Düllmann, L. Ghys, F. Heßberger, K. Hirose, H. Ikezoe, J. Khuyagbaatar, B. Kindler, B. Lommel, H. Makii, I. Nishinaka, T. Ohtsuki, S. Pain, R. Sagaidak, I. Tsekhanovich, M. Venhart, Y. Wakabayashi *et al.*, Phys. Lett. B **748**, 89 (2015).

[16] I. Tsekhanovich, A. N. Andreyev, K. Nishio, D. Denis-Petit, K. Hirose, H. Makii, Z. Matheson, K. Morimoto, K. Morita, W. Nazarewicz, R. Orlandi, J. Sadhukhan, T. Tanaka, M. Vermeulen, and M. Warda, Phys. Lett. B **790**, 583 (2019).

[17] C. Schmitt, A. Lemasson, K.-H. Schmidt, A. Jhingan, S. Biswas, Y. H. Kim, D. Ramos, A. N. Andreyev, D. Curien, M. Ciemala, E. Clément, O. Dorvaux, B. De Canditiis, F. Didierjean, G. Duchêne, J. Dudouet, J. Frankland, B. Jacquot, C. Raison, D. Ralet *et al.*, Phys. Rev. Lett. **126**, 132502 (2021).

[18] K. Mahata, C. Schmitt, S. Gupta, A. Shrivastava, G. Scamps, and K. H. Schmidt, Phys. Lett. B **825**, 136859 (2022).

[19] R. Vandenbosch and J. R. Huizenga, *Nuclear Fission* (Academic Press, New York, 1973).

[20] M. Warda, A. Staszczak, and W. Nazarewicz, Phys. Rev. C **86**, 024601 (2012).

[21] A. V. Andreev, G. G. Adamian, and N. V. Antonenko, Phys. Rev. C **93**, 034620 (2016).

[22] T. Ichikawa and P. Möller, Phys. Lett. B **789**, 679 (2019).

[23] G. Scamps and C. Simenel, Phys. Rev. C **100**, 041602(R) (2019).

[24] P. Möller and J. Randrup, Phys. Rev. C **91**, 044316 (2015).

[25] K.-H. Schmidt, B. Jurado, C. Amouroux, and C. Schmitt, Nucl. Data Sheets **131**, 107 (2016), Special Issue on Nuclear Reaction Data.

[26] S. Dhuri, K. Mahata, A. Shrivastava, K. Ramachandran, S. K. Pandit, V. Kumar, V. V. Parkar, P. C. Rout, A. Kumar, A. Chavan, S. Kaur, and T. Santhosh, Phys. Rev. C **106**, 014616 (2022).

[27] S. Gupta, K. Mahata, A. Shrivastava, K. Ramachandran, S. K. Pandit, P. C. Rout, V. V. Parkar, R. Tripathi, A. Kumar, B. K. Nayak, E. T. Mirgule, A. Saxena, S. Kailas, A. Jhingan, A. K. Nasirov, G. A. Yuldasheva, P. N. Nadtochy, and C. Schmitt, Phys. Lett. B **803**, 135297 (2020).

[28] M. G. Itkis, N. A. Kondratev, S. I. Mulgin, V. N. Okolovich, and Rusanov, Sov. J. Nucl. Phys. **52**, 601 (1990) [Yad. Fiz. 52, 944 (1990)].

[29] B. M. A. Swinton-Bland, M. A. Stoyer, A. C. Berriman, D. J. Hinde, C. Simenel, J. Buete, T. Tanaka, K. Banerjee, L. T. Bezzina, I. P. Carter, K. J. Cook, M. Dasgupta, D. Y. Jeung, C. Sengupta, E. C. Simpson, and K. Vo-Phuoc, Phys. Rev. C **102**, 054611 (2020).

[30] A. Jhingan, Pramana **85**, 483 (2015).

[31] A. Kumar, K. Ramachandran, A. Chatterjee, K. Mahata, V. V. Parkar, S. K. Pandit, and A. Shrivastava, *Proceedings of the DAE Symp. Phys. Nucl. Phys. held at Thapar Institute of Engineering & Technology, Patiala, Panjab, 2017*, edited by V. Jha, B. V. John and A. Saxena (Bhabha Atomic Research Centre, Mumbai, 2017), Vol. 62, p. 1060.

[32] R. K. Choudhury, A. Saxena, A. Chatterjee, D. V. Shetty, S. S. Kapoor, M. Cinausero, L. Corradi, E. Farnea, E. Fioretto, A. Gadea, D. Napoli, G. Prete, A. M. Stefanini, D. Bazzaco, S. Beghini, D. Fabris, G. Montagnoli, G. Nebbia, C. Rossi-Alvarez, F. Scarlassara *et al.*, Phys. Rev. C **60**, 054609 (1999).

[33] J. F. Ziegler, M. Ziegler, and J. Biersack, Nucl. Instrum. Methods Phys. Res. B **268**, 1818 (2010), 19th International Conference on Ion Beam Analysis.

[34] V. E. Viola, K. Kwiatkowski, and M. Walker, Phys. Rev. C **31**, 1550 (1985).

[35] A. Gavron, Phys. Rev. C **21**, 230 (1980).

[36] K. Mahata, S. Kailas, and S. S. Kapoor, Phys. Rev. C **92**, 034602 (2015).

[37] A. Chaudhuri, T. K. Ghosh, K. Banerjee, S. Bhattacharya, J. Sadhukhan, C. Bhattacharya, S. Kundu, J. K. Meena, G. Mukherjee, R. Pandey, T. K. Rana, P. Roy, T. Roy, V. Srivastava, and P. Bhattacharya, Phys. Rev. C **91**, 044620 (2015).

[38] A. V. Ignatyuk, G. N. Smirenkin, and A. S. Tishin, Sov. J. Nucl. Phys. **21**, 255 (1975) [Yad. Fiz. 21, 485 (1975)].

[39] P. C. Rout, D. R. Chakrabarty, V. M. Datar, S. Kumar, E. T. Mirgule, A. Mitra, V. Nanal, S. P. Behera, and V. Singh, Phys. Rev. Lett. **110**, 062501 (2013).

[40] M. G. Itkis and A. Y. Rusanov, Phys. Part. Nucl. **29**, 160 (1998).

[41] G. N. Knyazheva, E. M. Kozulin, R. N. Sagaidak, A. Y. Chizhov, M. G. Itkis, N. A. Kondratiev, V. M. Voskressensky, A. M. Stefanini, B. R. Behera, L. Corradi, E. Fioretto, A. Gadea, A. Latina, S. Szilner, M. Trotta, S. Beghini, G. Montagnoli, F. Scarlassara, F. Haas, N. Rowley *et al.*, Phys. Rev. C **75**, 064602 (2007).

[42] M. G. Itkis, N. A. Kondratev, S. I. Mulgin, V. N. Okolovich, and Rusanov, Sov. J. Nucl. Phys **53**, 757 (1991) [Yad. Fiz. 53, 1225 (1991)].